

Enhancing laser cutting quality of stainless steel 201 by controlling dross formation and surface roughness using multi-factor experimental design

Anwar Hassan Zabon¹, Tahseen Fadhil Abbas^{2*}, Aqeel Sabree Bedan¹ 

¹ Department of Production Engineering and Metallurgy, University of Technology, Baghdad, Iraq

² Department of Aeronautical Technical Engineering, College of Technical Engineering, Al-Farahidi University, Iraq

* Corresponding author's e-mail: tahseen.abbas@uofarahidi.edu.iq

ABSTRACT

A better process and products are thought to require characterization, evaluation of effects, and understanding of the damage extension caused by the laser cutting (LC) process on the surface integrity of the cut workpieces, given its many benefits and applications in the industry. In this work, 32-run CCD was used under response surface methodology (RSM) to examine the laser cutting of stainless steel 201 (SST 201) utilizing a 32-run experimental design. Laser power (Pu), cutting speed (V), frequency (F), focal position (FP), and gas pressure (P) are chosen as parameters for the input process, where the surface roughness and dross formation are taken into account as response variables in this process. Each parameter's relevance and impact was evaluated by a thorough statistical analysis that included Analysis of Variance (ANOVA), contour plots, main effect plots, and residual plots. The ANOVA results for surface roughness (Ra) and dross generated area (DA) are closely related since both are influenced by process parameters. While improving assist gas pressure enhances the surface quality and lowers the accumulation, increasing the laser power and cutting speed decreases both roughness and dross.

Keywords: fiber laser, dross formation, surface roughness, response surface method RSM, SST 201.

INTRODUCTION

With the invention of power lasers in the early 1970s, LC which is classified as an unconventional machining technique began to be used in the field. Due to its ability to create complicated forms, flexibility, speed, and the potential for high-quality finishing, LC is currently equivalent to the highest level of effectiveness and quality in the material cutting process. Laser material processing has emerged as an intriguing and competitive alternative to traditional manufacturing techniques in a number of industry categories [1]. Its high density and energy control, flexibility in the beam path, ease of raw material fixing, ease of automation, low emission pollution, fast speed, superb finishing W.P quality, a tiny HAZ (heat affect zone), a lack of contact,

and tool wear make it a beneficial method [2]. It is crucial to overcome obstacles, such as improving the surface polish, increasing the production rate, improving the accuracy, and extending the product life with a little negative influence on the society, environment, or machine workers [3]. Numerous process variables have a major impact on the quality of LC items. Many researches have looked into how these criteria affect the cut quality. Teixidor et al. (2012) conducted an investigation on the stainless steel (SS) fiber LC. For the impact on the cutting quality of peak pulse (Pu), F, and V for a given gas type and a gas pressure, the dimensions of the dross were represented mathematically [4]. Amaral et al. (2019) used a fiber laser to enhance and optimize the burr problem. In order to determine their significance for the cut surface quality, the

radiation Pu, V, and P were examined. It was discovered that a laser beam with higher cutting speed and less radiation power produced a better cut surface quality [5]. M. Sharifi et al. (2019) examined the impacts of V, Pu, T, and nozzle SOD, upon the cutting edge quality and cutting region temperature. AL6061-T6 alloy was laser-cut. The findings indicated that the most important component is Pu. [6, 7]. For the continuous CO₂ LC process, the effects of cutting Pu, V, and P variations on the workpiece's dross and Ra were examined via Zeilmann et al. (2022). It was determined that the primary variables influencing the production of burr and roughness during the LC process were V and P. [1]. Li1 et al. (2024) examined how the cutting quality of simulated fast reactor fuel rods was affected by the LC parameters of V, FP, Pu, and P. The results identified the best parameter values that balance the Ra, the cutting efficiency, and the least amount of slag production [8]. Alsaadawy et al. (2024) used the cutting parameters, including the laser Pu, V, and P; the parameters that had the biggest impact on the cutting quality were measured for surface roughness (Ra), kerf width (KW), Kerf taper (KT), and slag height Sh. The basic variables influencing the minimum slit taper and minimum slit width values were identified [9]. López1 et al. (2024) studied the effects of spot overlap and pulse energy upon the Ra and rear wall dross for AISI 316 L stainless steel minitube fiber LC. In order to evacuate the molten material, three treatments were compared: Compressed air, argon gas, and a control test. It was found that using compressed air or argon gas through tubes leads to a decrease in the back wall dross and dross height when compared to the control test [10, 11]. Genna et al. (2020) focused on how the laser beam cutting affects the kerf geometry, surface roughness, and cut edge quality in relation to the material type, workpiece, T (sheet thickness), V, and P. For every material, the ideal cutting circumstances

that meet the strict requirements of the chosen quality standard were found [12]. According to the studies evaluated in the literature of previous studies, the effect of Pu, V, F, T, P and Stand-off distance SOD, upon the surface integrity and dross formation was investigated. However, factors, such as Pu, V, P, FP, and F combined together have not received sufficient attention, leaving a research gap that requires further exploration. Therefore, this study was conducted to examine the influence of these parameters upon the dross formation and surface roughness.

EXPERIMENTAL PROCEDURES

The fiber laser IGR-3015F IGOLDEN CNC (computer numerical control) machine was utilized to carry out the studies. For every test, the focal point was consistently set at 10 mm, with a standoff distance of 0.5 mm, and air as the assist gas. A circular nozzle type single with a diameter of 3 mm was used, and the oxygen (O₂) was employed as the gas pressure. Table 1 contains comprehensive details on the mechanical and auxiliary supply devices.

The tests were fully programmed using conventional CNC programming. Figure 1 depicts the LC machine and its auxiliary supply components in general. The workpiece (W.P) material was austenitic stainless steel 201 having a (5 mm) thickness which is useful in many industries, including consumer products, automotive, architecture, kitchenware, and home utensils. The chemical composition of the material is provided in Table 2.

The alloy was cut using water jet process (WJM) into 32 equally sized samples, each measuring 50 × 40 × 5 mm, ensuring that the notch previously made by the fiber laser cutting (LC) process was positioned in the middle of each sample. The notch was produced at a length of 3.5 cm, as shown in Figure 2.

For laser metal cutting, five important controllable process parameters were taken into

Table 1. The fiber laser system used for the experiment and its specific features

| Parameters | Symbol | Values units | Units |
|-------------------|--------|-----------------|-------|
| Max. power | pu | 12000 | watt |
| Max. cutting size | | 3000 × 1500 | mm |
| Wavelength | λ | 1083 ± 3 | nm |
| Mode of operation | - | Continuous wave | - |
| Duty cycle | DC | 100 | - |
| Lens focal length | l | 127 | mm |

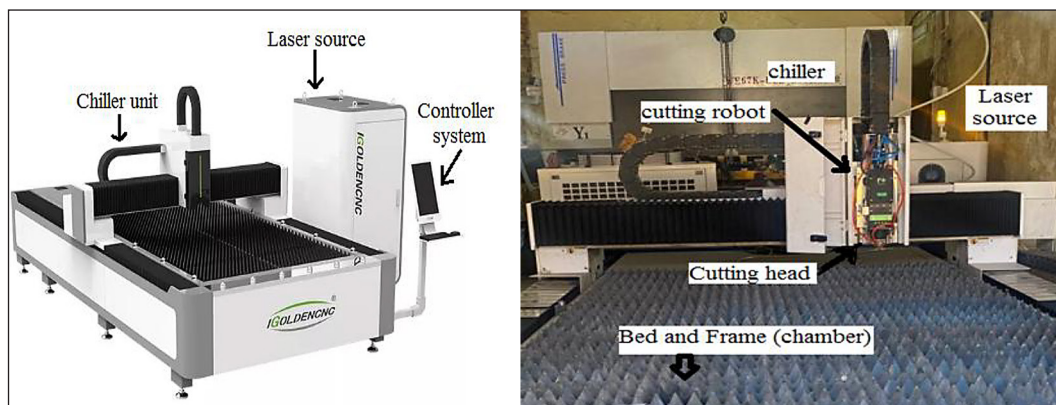


Figure 1. The general view of the laser cutting machine

Table 2. Chemical composition (wt.%) and the ASM standard for stainless steel 201

| Element | C% | Si% | Mn% | P% | Cr% | Mo% | Ni% | Cu% | Al% |
|----------|-------|-------|---------|---------|---------|--------|---------|-------|--------|
| Weight % | 0.136 | 0.219 | 5 | <0.0005 | 16 | <0.002 | 4.09 | 0.284 | <0.001 |
| ASM | 0.15 | 1 | 5.5–7.5 | 0.060 | 16 - 18 | - | 3.5–5.5 | - | - |

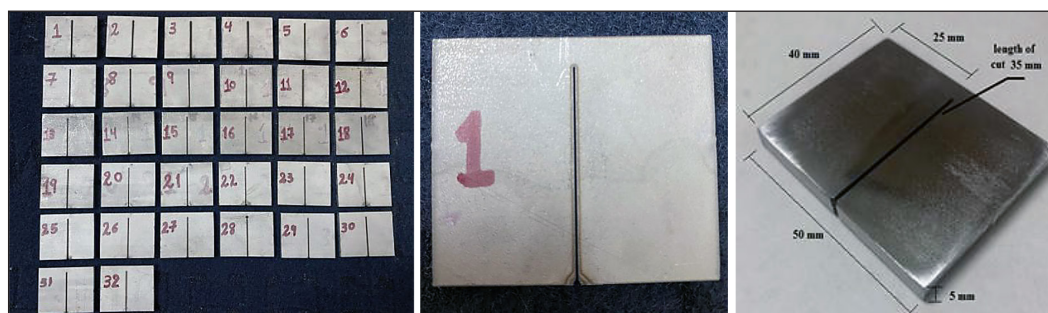


Figure 2. Samples (a) with created by WJM, (b) with central notch created by fiber LC, (c) with dimensions

consideration at three levels: Frequency (100, 2550, and 5000 Hz), focus position (FP) (-25, -12, and 1 mm), assist gas pressure (7, 10, and 13) bar, laser power (2000, 6000, and 10,000 Watt), and cutting speed (0.5, 1, and 1.5 m/min). The best collection of process parameters, as well as their ranges, must be chosen. These were chosen based on prior research and early experimental testing. Minitab V16, a statistical tool, was used to define the experimental run in line with RSM in order to minimize the number of experiments and accurately model and optimize the process. A five-factor, three-level central composite design (CCD) experimental schedule with six central points and 26 non-central points was used in this study, resulting in a total of 32 tests. Main effect plots, contour plots, ANOVA, and residual plots were used to analyze the output responses and the impact of input variables on the output responses.

MEASUREMENT OF CUTTING QUALITY

Two quality indices, including dross area (DA) and surface roughness (Ra) were employed. It was necessary to keep all parameters under strict control. The laser machine was equipped with various measuring devices to permit detailed examination of the interrelationship between the main process parameters.

Dross measurement

The term DA describes the molten material that is not kept out of the machining zone by gas flow and re-solidifies at the specimen's bottom. During the laser beam's passage, a residue is formed that drags the non-melting material and deposits it at the margins of the cut surfaces. Figure 3 displays a sample that had a dross flaw; extra

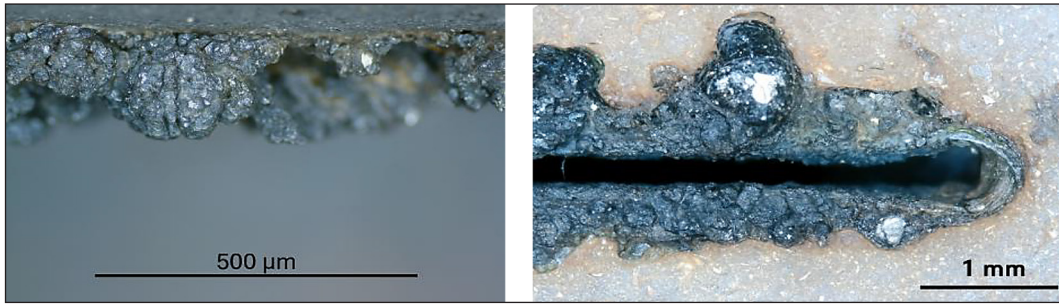


Figure 3. Sample with the defect of dross. (a) side view (b) top view

material was produced from the cut surface's bottom up [13]. The amount of dross accumulated on the lower edge of the pieces was evaluated after the process, by analyzing the area covered by the slag in relation to the total length of the pieces. ImageJ 1.48v software, an open-source image analysis tool, was employed to measure the dross area accumulated on the surface of the sample after laser cutting. The software enables accurate and efficient analysis of digital images. The captured images of the cut surfaces were imported into the program and then converted into high-contrast images to clearly define the edges. Subsequently, the measurement tools within the software were used to calculate the dross area along the cut edge. This method provided precise measurements of the dross area for each sample, allowing for a detailed analysis of the relationship between process variables and dross formation [14, 15], as shown in Figure 4. For calibration, the scale (known distance) that came with the figure was changed to the image's pixel distance. Measurements of various entities in the figure were made using the calibrated pixel distance as a guide. The pixels encircled by the space zone could also be used to calculate the dross area.

Ultimately, the relevant region for dross may be identified by comparing the contained pixels to the calibrated pixel [16].

Measurement of the surface roughness

For the purpose of measuring surface roughness and due to the difficulty of reaching the surface to be measured, samples were cut starting from a height of 10 mm from the lower edge of each sample horizontally, all the way to the laser cutting slit. This resulted in a rectangular cut with the same dimensions for all samples in the manner evinced in Figure 5.

The samples were cut in wire electrical discharge machining, which does not generate heat to ensure that the samples are not thermally affected. The surface roughness of the machined surface is measured using the average Ra parameter. The vertical dimensions of roughness are described by the arithmetic average height of surface component (profile) abnormalities from the mean line within the measuring length [17, 18].

Figure 6 manifests the Ra Tester Pocket Surf device from Mahr Company a Mahr® M2 portable equipment, MarSurf® has a measurement

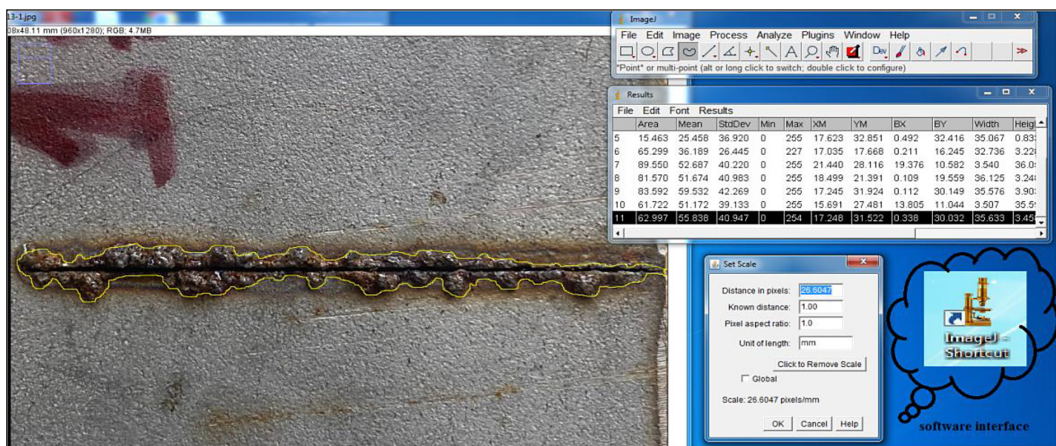


Figure 4. Measurement of the dross area using ImageJ

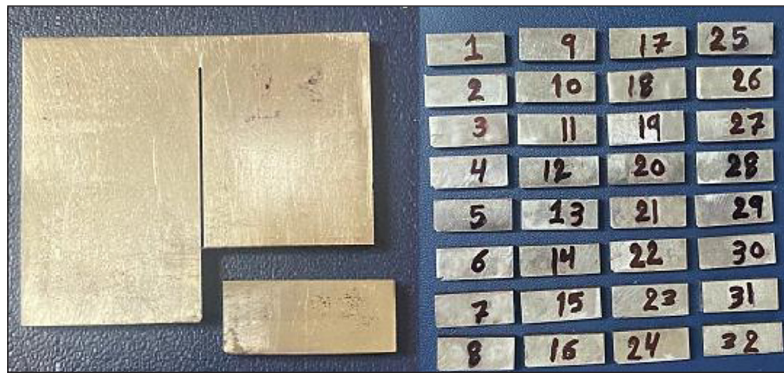


Figure 5. A sample cut in the EDM (electrical discharge machining)

accuracy of approximately $\pm 0.01 \mu\text{m}$. Three measurements of the various roughness metrics were conducted on the faiber LC machined area using software, and the average value was utilized to record and capture the roughness values; the unit of measure is μm . All surface roughness measurements were carried out over a 10 mm evaluation length. Three readings were taken at equally spaced intervals along the measured surface, and the average value was recorded. The measurement followed ISO 4288 standards using a Gaussian filter to ensure consistent and representative roughness values.

Finally, the measured values of Ra and DA in relation to the input machining factors are displayed in Table 3. The statistical program Minitab (Version V17, Gandhinagar, India) was utilized to analyze these measured responses. Regression analysis was used to determine mathematical relationships between each response variable and the machining parameters.

RESULT AND DISCUSSION

Dross analysis

The importance of the input variables in relation to the created model was examined using the ANOVA technique for dross, as indicated in Table 4. The dross area ANOVA results show that the p-values are less than 0.05. The model appears to suit the available data based on the R-sq. and R-sq. (adj.) values.[19, 20].

Model summary

S = 0.0076750, R-sq. = 99.04%,
R-sq(adj) = 97.29%, R-sq(pred) = 23.10%.

Regression equation in uncoded units – the data demonstrate how significant the dross deposition is. In order to forecast the size of this dross as a function of certain LC parameters, a mathematical model is therefore developed by doing



Figure 6. The Ra tester pocket surf device

Table 3. Experimental values of SR and DA in micrometer based on RSM technique

| Run # | (Pu) watt | (V) mm/min | (P) bar | (F) Hz | (FP) mm | (DA) mm ² | (Ra) μm |
|-------|-----------|------------|---------|--------|---------|----------------------|---------|
| 1 | 10000 | 1.5 | 7 | 100 | 1 | 15.573 | 5.810 |
| 2 | 2000 | 0.5 | 7 | 100 | 1 | 111.290 | 3.064 |
| 3 | 2000 | 1.5 | 13 | 100 | 1 | 68.354 | 5.100 |
| 4 | 6000 | 1.0 | 10 | 2550 | 1 | 44.020 | 5.032 |
| 5 | 6000 | 1.0 | 7 | 2550 | -12 | 98.052 | 4.950 |
| 6 | 6000 | 1.0 | 10 | 2550 | -12 | 71.573 | 5.191 |
| 7 | 2000 | 1.5 | 13 | 5000 | -25 | 110.090 | 7.209 |
| 8 | 10000 | 1.0 | 10 | 2550 | -12 | 44.344 | 5.110 |
| 9 | 10000 | 1.5 | 13 | 5000 | 1 | 14.757 | 6.020 |
| 10 | 6000 | 1.0 | 10 | 5000 | -12 | 44.853 | 5.990 |
| 11 | 6000 | 1.0 | 10 | 2550 | -12 | 61.954 | 5.159 |
| 12 | 2000 | 0.5 | 13 | 5000 | 1 | 27.623 | 3.110 |
| 13 | 6000 | 0.5 | 10 | 2550 | -12 | 84.269 | 1.780 |
| 14 | 2000 | 0.5 | 7 | 5000 | -25 | 100.807 | 4.890 |
| 15 | 6000 | 1.0 | 13 | 2550 | -12 | 48.620 | 5.430 |
| 16 | 6000 | 1.0 | 10 | 2550 | -12 | 71.954 | 5.258 |
| 17 | 2000 | 0.5 | 13 | 100 | -25 | 93.489 | 3.890 |
| 18 | 6000 | 1.0 | 10 | 2550 | -12 | 75.547 | 4.940 |
| 19 | 10000 | 0.5 | 7 | 100 | -25 | 79.636 | 3.037 |
| 20 | 10000 | 1.5 | 13 | 100 | -25 | 105.230 | 4.460 |
| 21 | 2000 | 1.0 | 10 | 2550 | -12 | 120.840 | 5.620 |
| 22 | 2000 | 1.5 | 7 | 100 | -25 | 75.076 | 5.470 |
| 23 | 2000 | 1.5 | 7 | 5000 | 1 | 35.483 | 4.870 |
| 24 | 10000 | 0.5 | 13 | 100 | 1 | 16.829 | 4.049 |
| 25 | 6000 | 1.0 | 10 | 2550 | -25 | 85.240 | 5.220 |
| 26 | 10000 | 1.5 | 7 | 5000 | -25 | 21.960 | 5.144 |
| 27 | 10000 | 0.5 | 7 | 5000 | 1 | 62.360 | 3.800 |
| 28 | 6000 | 1.0 | 10 | 2550 | -12 | 72.632 | 5.600 |
| 29 | 10000 | 0.5 | 13 | 5000 | -25 | 38.064 | 3.270 |
| 30 | 6000 | 1.5 | 10 | 2550 | -12 | 55.210 | 4.938 |
| 31 | 6000 | 1.0 | 10 | 100 | -12 | 70.197 | 5.355 |
| 32 | 6000 | 1.0 | 10 | 2550 | -12 | 71.752 | 4.960 |

this, one can choose the ideal laser settings to lower the quantity of dross.

$$\begin{aligned}
 DA^{0.5} = & 0.0570 - 0.000003P_u - 0.1482V - 0.0149P + \\
 & + 0.000025F + 0.001847FP - 0.0000P_u \times P_u - \\
 & - 0.0121V \times V - 0.000385P \times P - 0.000000F \times F - \\
 & - 0.000064FP \times FP - 0.000005P_u \times V - 0.000000P_u \times \\
 & \times P + 0.000000 P_u \times F - 0.000000 P_u \times FP + \\
 & + 0.01844V \times P - 0.000006 V \times F - 0.000987 V \times \\
 & \times FP - 0.000001 P \times F - 0.000408 P \times FP + \\
 & + 0.000000 F \times FP \tag{1}
 \end{aligned}$$

The residual graphs for the dross area are shown in Figure 7. Residual plotting is essential to confirm the validity of the outcomes of the ANOVA. The four-in-one residual plots verify the

adequacy of the model. For a normal distribution, the normal probability plot displays a straight line. The residual vs. fitted figure shows that the residuals are distributed randomly, confirming the assumptions of the ANOVA. The parabolic form of the histogram verifies the normalcy. ANOVA reliability is ensured when there are no trends in the residual vs. fitted plot [21, 22].

According to the ANOVA results, laser power had the biggest impact contributing 45%, followed by focus position at 39% and laser speed at 7%. Additionally, frequency had the contribution 6.3%, and gas pressure had the minimal contribution 2.7%. These findings suggest that the current

Table 4. ANOVA for dross area

| Source | DF | Adj SS | Adj MS | F-Value | P-Value | VIF |
|-------------------|----|----------|----------|---------|---------|------|
| Liner | 5 | 0.036140 | 0.007228 | 122.71 | 0.000 | |
| pu | 1 | 0.016243 | 0.016243 | 275.74 | 0.000 | 1.00 |
| V | 1 | 0.002620 | 0.002620 | 44.48 | 0.000 | 1.00 |
| P | 1 | 0.000981 | 0.000981 | 16.65 | 0.002 | 1.00 |
| F | 1 | 0.002315 | 0.002315 | 39.31 | 0.000 | 1.00 |
| FP | 1 | 0.013981 | 0.013981 | 237.35 | 0.000 | 1.00 |
| 2-Way Interaction | 10 | 0.022719 | 0.002272 | 38.57 | 0.000 | |
| Pu × V | 1 | 0.001776 | 0.001776 | 30.16 | 0.000 | 1.00 |
| Pu × P | 1 | 0.000042 | 0.000042 | 0.71 | 0.417 | 1.00 |
| Pu × F | 1 | 0.000246 | 0.000246 | 4.18 | 0.066 | 1.00 |
| Pu × FP | 1 | 0.001207 | 0.001207 | 20.48 | 0.001 | 1.00 |
| V × P | 1 | 0.012237 | 0.012237 | 207.74 | 0.000 | 1.00 |
| V × F | 1 | 0.000978 | 0.000978 | 16.60 | 0.002 | 1.00 |
| V × FP | 1 | 0.000659 | 0.000659 | 11.18 | 0.007 | 1.00 |
| P × F | 1 | 0.000763 | 0.000763 | 12.96 | 0.004 | 1.00 |
| P × FP | 1 | 0.004056 | 0.004056 | 68.86 | 0.000 | 1.00 |
| F × FP | 1 | 0.000754 | 0.000754 | 12.80 | 0.004 | 1.00 |

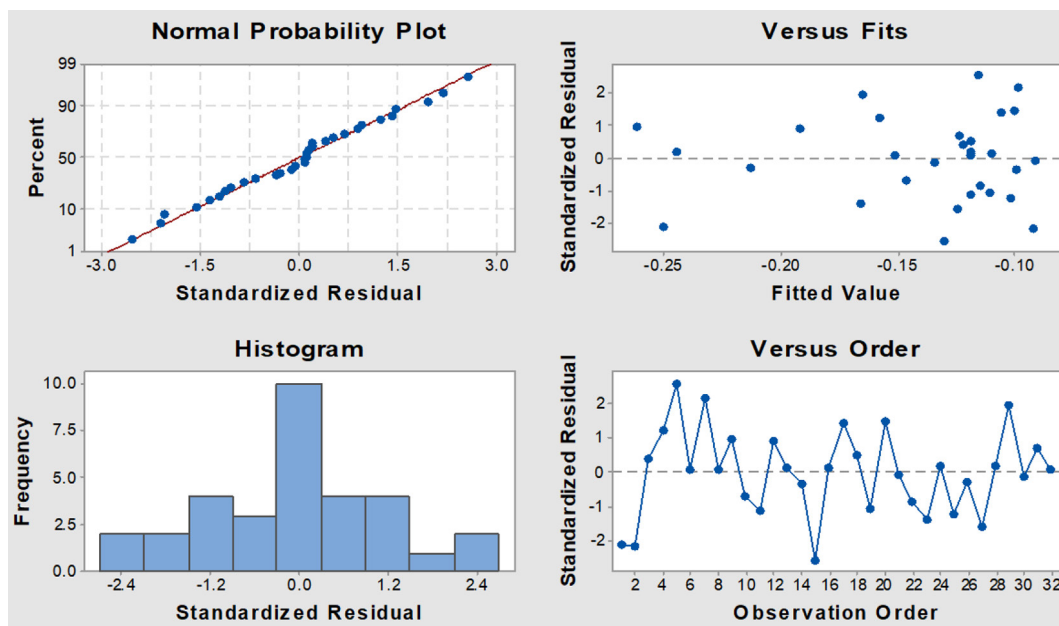


Figure 7. Residual plots for the dross area

study provides a solid foundation for future estimations and analyses. Figure 8 illustrates the proportional contribution of each machining parameter to DA through variation from the mean value of dross is significantly smaller.

Figure 9 demonstrates the impact of machining factors on the DA, offering insights for optimizing the cutting processes to improve the product quality. Increasing Pu and V reduces the DA, as

the higher power enhances the material removal, and the faster speeds minimize the excessive melting. Higher assist gas pressure slightly decreases the dross, improving the molten material ejection. Frequency depicts a nonlinear effect, and initially increasing the dross before optimizing the removal at a certain level excessive frequency may cause instability. A more negative focus position (-25) leads to more dross, while a focus closer to zero

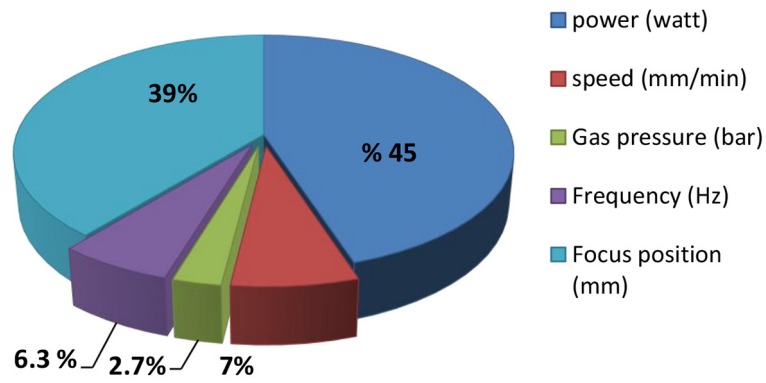


Figure 8. The percentage that machining factors contribute to DA

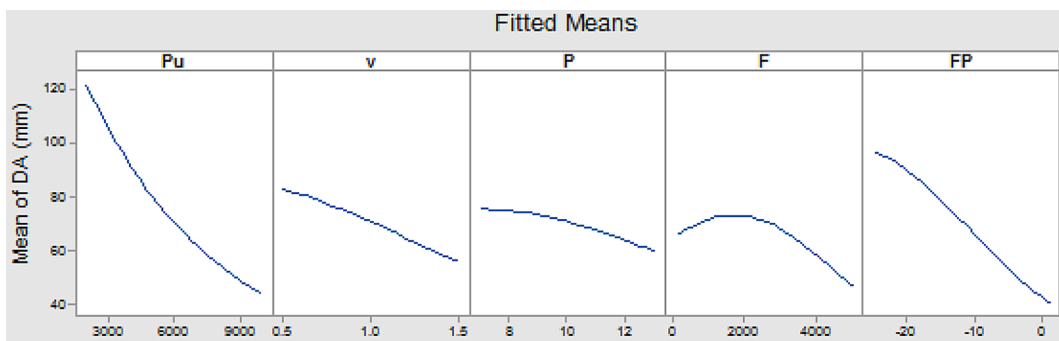


Figure 9. Effects of the machining parameters on the DA

enhances the precision and reduces the heat-affected zones. Figure 10 portrays the contour plots which illustrate the effect of machining parameters on the dross area in LC. Each plot shows the interaction of two parameters while keeping others

constant. Higher laser power and cutting speed significantly reduce the dross, as the prolonged exposure at low speeds leads to excessive melting. Increased gas pressure improves the molten material ejection, minimizing the dross. Moderate

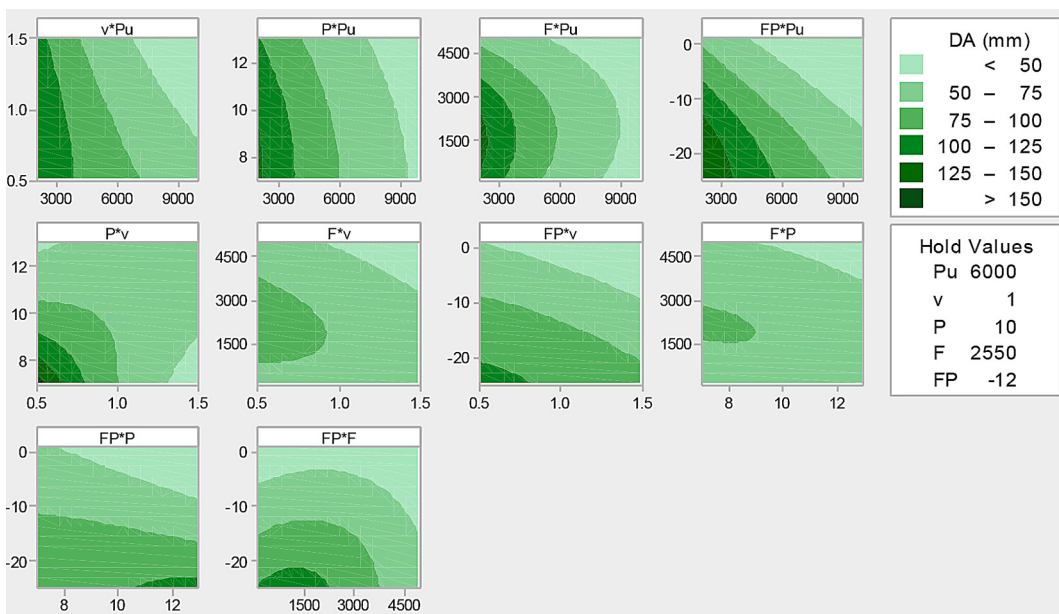


Figure 10. The contour plots of dross area

frequency optimizes the material removal, while too low or too high frequencies increase the dross. A focus position near zero enhances the precision and reduces the dross, whereas a highly negative focus position (-25 or lower) results in inefficient energy distribution and more dross. High speed and high pressure minimize the dross, while the low speed, low pressure, and extreme focus positions lead to increased accumulation.

In Figure 11, the samples with the lowest and greatest dross areas are displayed. It is obvious that there was dross in the treated samples. Not all of the molten material was discharged from the cut kerf and adhered to the cut wall's bottom side. It illustrates that the higher laser power, moderate to high V, and increased P contribute to reducing dross formation, while the lower power and slower cutting speeds lead to greater dross accumulation.

Analysis of surface roughness (Ra)

In the same way, the significance of the chosen input variable was examined using the ANOVA

approach. Table 5 displays the Ra's ANOVA results. It demonstrates that every machining parameter significantly affects the Ra. Less than 20% of the difference between the R-sq. and Adjusted (Adj.) R-sq. values suggests that the current model is appropriate and capable of offering the best fit for the available data [14]

Model summary

S = 2.11937, R-sq. = 98.31%,
R-sq(adj) = 95.22%, R-sq(pred) = 45.67%.

Regression equation in uncoded units:

$$Ra^2 = -25.5 + 0.00055Pu + 108.1V - 1.78P - 0.00721F - 0.527FP + 0.000000Pu \times Pu - 50.97V \times V + 0.053P \times P + 0.000001F \times F - 0.00139FP \times F - 0.000247Pu \times V - 0.000086Pu \times P - 0.0000Pu \times F + 0.000104Pu \times FP + 1.055V \times P + 0.001032V \times F + 0.0053V \times FP + 0.000212P \times F - 0.0018P \times FP - 0.000079 F \times FP \quad (2)$$

The residual graphs for the Ra are exhibited in Figure 12. Residual plotting is essential to confirm the validity of the ANOVA results. The four-in-one

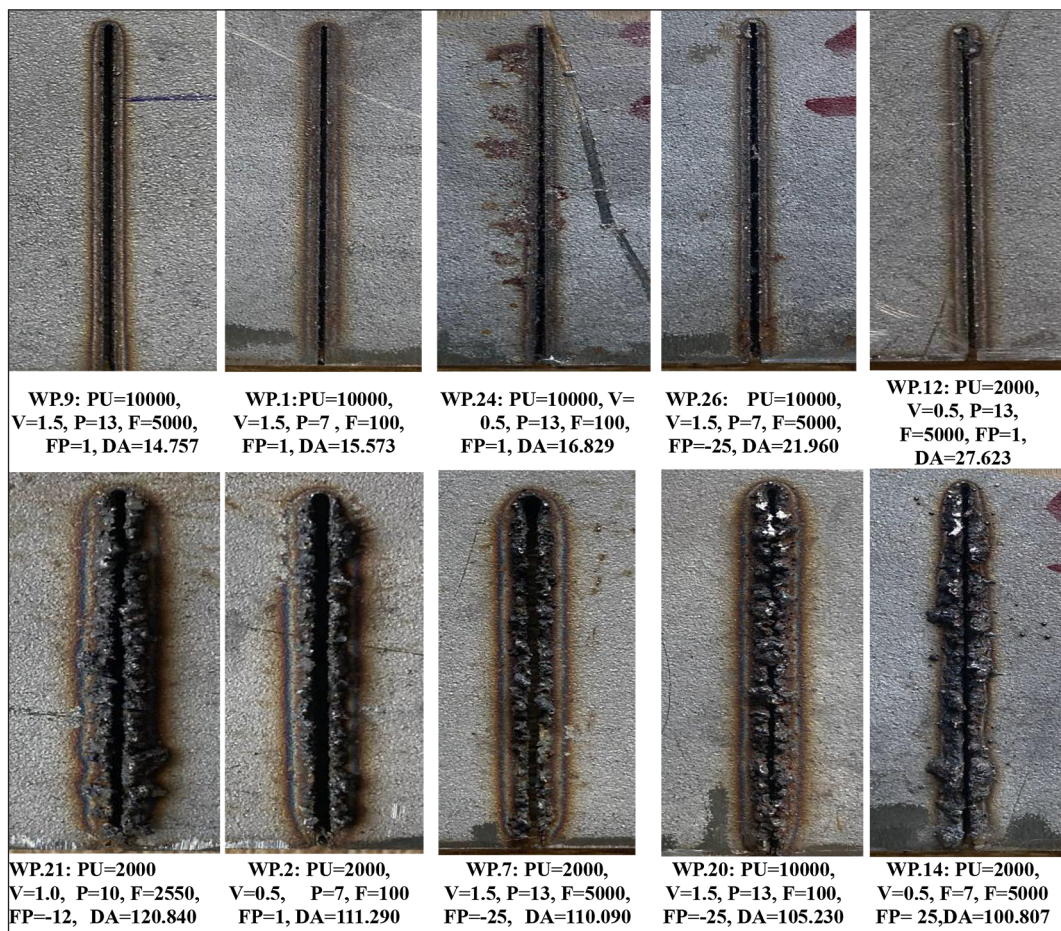


Figure 11. Pictures of the samples that recorded the lowest and maximum values of DA

Table 5. ANOVA for surface roughness area

| Source | DF | Adj SS | Adj MS | F-Value | P-Value | VIF |
|-------------------|----|---------|---------|---------|---------|------|
| Liner | 5 | 1626.11 | 325.22 | 72.40 | 0.000 | |
| pu | 1 | 43.85 | 43.85 | 9.76 | 0.010 | 1.00 |
| V | 1 | 1428.04 | 1428.04 | 317.93 | 0.000 | 1.00 |
| P | 1 | 22.60 | 22.60 | 5.03 | 0.046 | 1.00 |
| F | 1 | 110.47 | 110.47 | 24.59 | 0.000 | 1.00 |
| FP | 1 | 21.15 | 21.15 | 4.71 | 0.053 | 1.00 |
| 2-Way Interaction | 10 | 722.78 | 72.28 | 16.09 | 0.000 | |
| Pu × V | 1 | 3.92 | 3.92 | 0.87 | 0.371 | 1.00 |
| Pu × P | 1 | 17.03 | 17.03 | 3.79 | 0.077 | 1.00 |
| Pu × F | 1 | 25.63 | 25.63 | 5.71 | 0.036 | 1.00 |
| Pu × FP | 1 | 469.91 | 469.91 | 104.62 | 0.000 | 1.00 |
| V × P | 1 | 40.10 | 40.10 | 8.93 | 0.012 | 1.00 |
| V × F | 1 | 25.58 | 25.58 | 5.69 | 0.036 | 1.00 |
| V × FP | 1 | 0.02 | 0.02 | 0.00 | 0.950 | 1.00 |
| P × F | 1 | 38.77 | 38.77 | 8.63 | 0.013 | 1.00 |
| P × FP | 1 | 0.08 | 0.08 | 0.02 | 0.894 | 1.00 |
| F × FP | 1 | 101.74 | 101.74 | 22.65 | 0.001 | 1.00 |

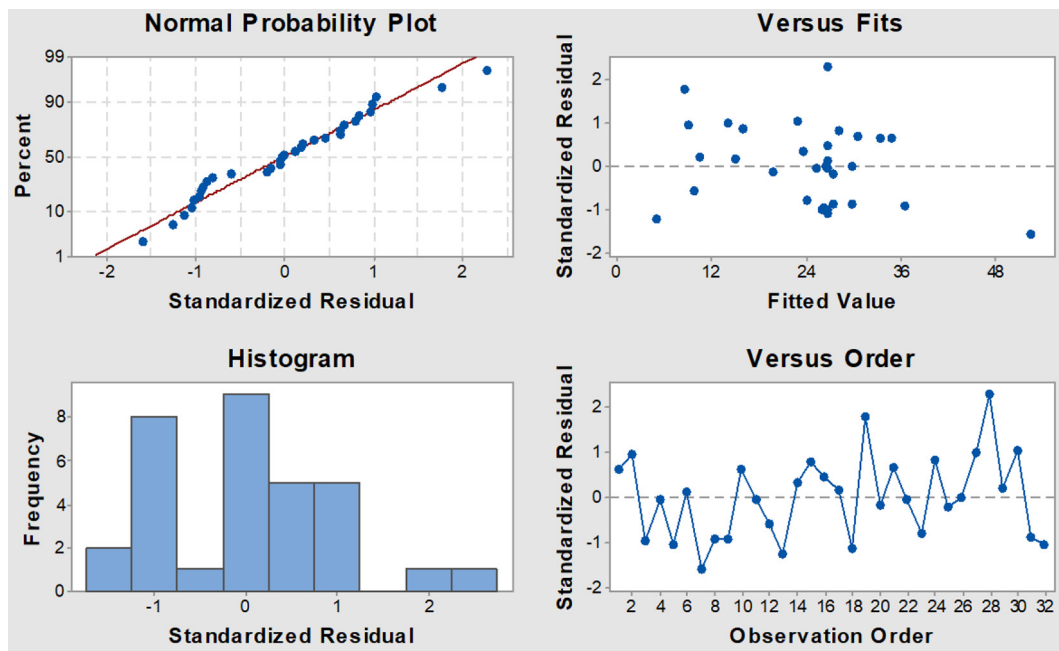


Figure 12. Residual plots for surface roughness

residual plots verify the adequacy of the model: For a normal distribution, the normal probability plot displays a straight line. The residual vs. fitted figure indicates that the residuals are distributed randomly, confirming the assumptions of the ANOVA. The parabolic form of the histogram verifies the normalcy. ANOVA reliability is ensured when there are no trends in the residual vs. fitted plot [16, 17]. Figure 13 displays a pie chart that

illustrates the machining variables’ proportional contribution to Ra. According to the ANOVA results, the highest was the cutting speed with 87.8% contribution followed by the frequency with 6.8% contribution, and the power with 2.7% contribution was observed. Additionally, the focal position and gas pressure had minimal contribution with 1.3% and 1.4%, respectively, indicating that the present study could be effectively used as a basis

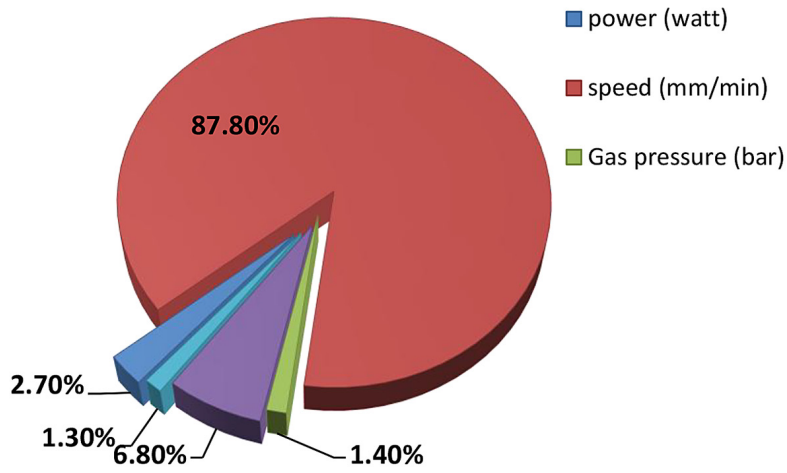


Figure 13. The percentage that machining factors contribute to Ra

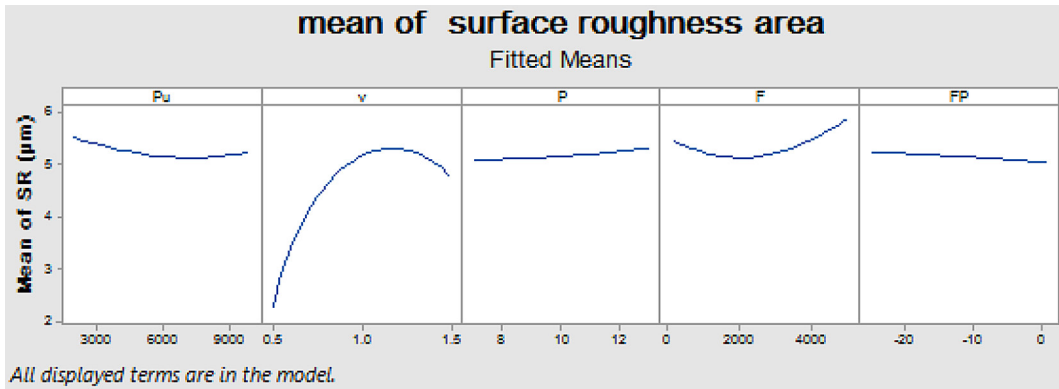


Figure 14. Effects of the machining parameters on Ra

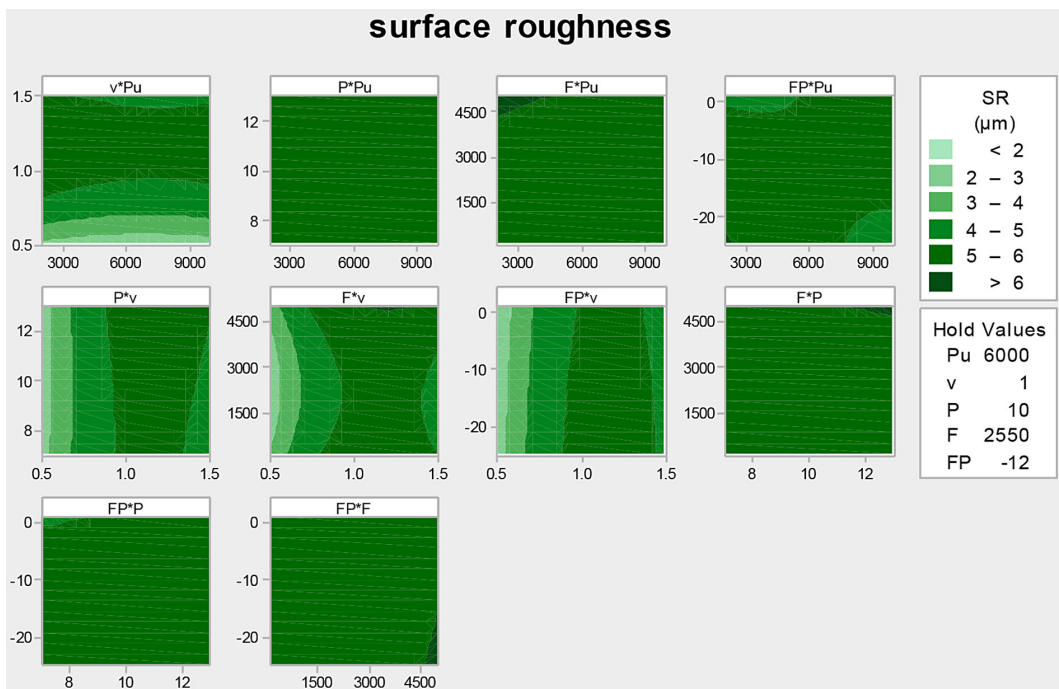


Figure 15. Contour plots on Ra

for future predictions. The observed standard deviation for Ra was 2.11937, indicating the highest possible variation from the mean value.

The Figure 14 reveals the effect of LC parameters on the Ra. Increasing the laser power reduces the roughness, while the cutting speed has a curvilinear effect, with roughness increasing at medium speeds and then decreasing. Gas pressure and frequency have a significant effect on the roughness, with optimum values for each. Focus position has a slight effect. These results reflect the importance of tuning parameters to achieve the best surface quality. The Figure 15 illustrates the effect of two-factor interactions on the surface roughness (Ra) in laser cutting using color maps. Lighter shades indicate lower roughness, while darker shades represent higher roughness. It is observed that certain interactions, such as laser power with cutting speed, have a significant impact on the roughness, whereas the other parameters show the minimal influence. These findings highlight the importance of optimizing the key parameters to achieve better surface quality.

These findings are consistent with those reported by Teixidor et al. [4], who also found that increasing laser power and cutting speed reduces dross formation. Similarly, Amaral et al. [5] observed that surface roughness decreases with optimized assist gas pressure. The trends in our study align well with Zeilmann et al. [1], particularly regarding the influence of cutting speed and gas pressure. Our results also support Singh et al. [15], who highlighted the importance of proper focus and gas dynamics in minimizing dross.

CONCLUSIONS

The present investigation examined the effects of various fiber LC process parameters, comprising assist gas pressure, frequency, laser power, cutting speed, and focal position on the DA and Ra in 201 stainless steel. The following key findings are drawn from the study:

Based on the ANOVA results for the DA, three machining factors were identified as significant: Laser power had the biggest impact contributing 45%, followed by focus position at 39% and Laser speed at 7%. While the contributions of the remaining factors were minimal: frequency at 6.3% and gas pressure at 2.7 %.

Higher Pu, V, and P help reduce the dross formation. F and FP have a significant impact, requiring fine-tuning to avoid excessive dross.

To minimize dross formation, higher power, increased cutting speed, optimized assist gas pressure, and proper frequency settings are recommended. Moreover, Focus position plays a crucial role in controlling the dross and needs fine-tuning.

The ANOVA results for the Ra demonstrate the contribution of V was the highest with 87.8%, then F with 6.8% contribution, and Pu with 2.7% contribution was observed. Additionally, focal position and gas pressure had minimal contribution, with 1.3% and 1.4% respectively.

The six central points in the CCD design were included specifically to assess the repeatability and consistency of the experimental results. The variation among the central points was analyzed statistically using ANOVA, and the results showed minimal variation, confirming good repeatability.

Increasing laser power reduces surface roughness. Cutting speed has a nonlinear effect, where the roughness increases at medium speeds and then decreases at higher speeds. Gas pressure and frequency significantly influence the roughness, with optimal values for each to achieve better surface quality. In contrast, focus position has a minor effect compared to other parameters.

Surface roughness and dross generation are closely related since both are influenced by process parameters. While improving the assist gas pressure enhances the surface quality and lowers the accumulation, as well as increasing the Pu and V decreases both roughness and dross. Additionally, the important parameters are frequency and focal position, since the incorrect settings can make the dross and roughness worse. Consequently, in order to attain the best cutting quality, a careful control of these factors is necessary.

REFERENCES

1. Zeilmann R.P. and Conrado R. D., Effects of cutting power, speed and assist gas pressure parameters on the surface integrity cut by laser, *Procedia CIRP*, 2022, 108, C, 367–371, doi: 10.1016/j.procir.2022.03.060.
2. Al-Thamir M., Algodí S. J., Al-Hamdani K. S., Abed A. A. The effect of nominal powder thickness on solidification behavior of atypical multilayer WC–Co components fabricated by laser-powder bed fusion. *Springer Nature*, 2024, 9, 237–245, doi: 10.1007/s40964-023-00445-4.

3. Vora J. et al., Experimental investigations and pareto optimization of fiber laser cutting process of Ti6AL4V, *Metals (Basel)*, 2021, 11(9), 1–27, doi: 10.3390/met11091461.
4. Teixidor D., Ciurana J., and Rodriguez C. A. Dross formation and process parameters analysis of fibre laser cutting of stainless steel thin sheets, *Int. J. Adv. Manuf. Technol.*, 2014, 71(9–12), 1611–1621, doi: 10.1007/s00170-013-5599-0.
5. Amaral I., Silva F. J. G., Pinto G. F. L., Campilho R. D. S. G., and Gouveia R. M. Improving the cut surface quality by optimizing parameters in the fibre laser cutting process, *Procedia Manuf.*, 2019, 38, 1111–1120, doi: 10.1016/j.promfg.2020.01.199.
6. Sharifi M. and Akbari M. Experimental investigation of the effect of process parameters on cutting region temperature and cutting edge quality in laser cutting of AL6061T6 alloy, *Optik (Stuttg)*, February 2019, 184, 457–463, doi: 10.1016/j.ijleo.2019.04.105.
7. Bedan A. S., Shabeeb A. H. and Hussein E. A. Improve single point incremental forming process performance using primary stretching forming process, *Advance in Science and Technology Research Journal*, 2023, 17(5), 260–268, doi: 10.12913/22998624/172907.
8. Li T. et al. Experimental study on laser cutting process of simulated fast Reactor fuel rods, *Sci. Rep.*, 2024, 14(1), 1–12, doi: 10.1038/s41598-024-81161-z.
9. Alsaadawy M., Dewidar M., Said A., Maher I., and Shehabeldeen T. A. Investigation of the effect of laser cutting parameters on surface and kerf quality of thick Ti–6Al–4V alloy sheets, *Arab. J. Sci. Eng.*, 2024, doi: 10.1007/s13369-024-09083-6.
10. García-López E., Siller H., Vazquez-Lepe E., Ramirez-Galindo J. G., and Rodriguez C. A. Minimizing surface roughness and back wall dross for fiber laser micro-cutting on AISI 316 L tubes using response surface methodology, *Mater. Res. Express*, 2024, 11(2), 0–13, doi: 10.1088/2053-1591/ad215c.
11. Jasim A. N., Mohammed A., Mustafa A. M., Sayyid F. F., Aljibori H. S., Al-Azzawi W. K., Al-Amiery A. A., and Yousif E. A. Corrosion inhibition of mild steel in HCl solution by 2-acetylpyrazine: Weight loss and DFT studies on immersion time and temperature effects. *Progress in Color, Colorants and Coatings* 2024, 17(4), 333–350. doi:10.30509/PCCC.2024.167231.1261.
12. Genna S., Menna E., Rubino G., and Tagliaferri V. Experimental investigation of industrial laser cutting: The effect of the material selection and the process parameters on the kerf quality, *Appl. Sci.*, 2020, 10(14), doi: 10.3390/app10144956.
13. Cavusoglu O. The 3D surface morphological investigation of laser cutting process of 2024-T3 aluminum alloy sheet, *Optik (Stuttg)*, March 2021, 238, 166739, doi: 10.1016/j.ijleo.2021.166739.
14. Pacher M., Franceschetti L., Strada S. C., Tanelli M., Savaresi S. M., and Previtali B. Real-time continuous estimation of dross attachment in the laser cutting process based on process emission images, *J. Laser Appl.*, 2020, 32(4), doi: 10.2351/7.0000145.
15. Singh A. K., Bal K. S., Pal A. R., Dey D., and Roy Choudhury A. A novel method to reduce dross in laser beam cutting of Ti-6Al-4 V alloy sheet, *J. Manuf. Process.*, 2021, 64, 95–112, doi: 10.1016/j.jmapro.2021.01.020.
16. Al-Ghuraibawi, A., Abed, A. H., Mansor, K. K. Numerical simulation of forming a 3D shape by a multi-point die simulaci3n Salud, Ciencia y Tecnologia - Serie de Conferencias, 2024, 36, doi: 10.56294/sctconf2024848.
17. Ghazi, S. K., Salloom, M. Y., Bedan, A. S. Experimental evaluation of a system to control the incremental forming of aluminum alloy type 1050, *Engineering, Technology and Applied Science Research*, 2024, 14(5), 16943–16949, doi:10.48084/etasr.8387.
18. Patidar D. and Rana R. S. The effect of CO₂ laser cutting parameter on Mechanical & Microstructural characteristics of high strength steel-a review, *Mater. Today Proc.*, 2018, 5(9), 17753–17762, doi: 10.1016/j.matpr.2018.06.099.
19. Khalida K. Mansor E. A. H. F. A., Bedan A. S., Mansor S. A. H. A Statistical Investigation and Prediction of the Effect of FDM Variables on Flexural Stress of PLA Prints, 2024, 31(3), 10–17.
20. Al-Ghuraibawi, A., Abed, A. H., Mansor, K. K. Simulation and experimental approach for metal forming with a multi-point die. *Salud, Ciencia y Tecnologia - Serie de Conferencias*, March 2024, 36 doi: 10.56294/sctconf2024855.
21. Abtan N. S., Sultan A. E., Sayyid F. F., Alamiery A. A., Jaz A. H., Gaaz T. S., Ahmed S. M., Mustafa A. M., Ali D. A. and Hanoon M. M. Enhancing corrosion resistance of mild steel in hydrochloric acid solution using 4-phenyl-1-(phenylsulfonyl)-3-thiosemicarbazide: A comprehensive study, *Int. J. Corros. Scale Inhib.*, 2024, 13(1), 435–459. doi: 10.17675/2305-6894-2024-13-1-22.
22. Chaudhari R., Vora J., de Lacalle L. N. L., Khanna S., Patel V. K., and Ayesta I. Parametric optimization and effect of nano-graphene mixed dielectric fluid on performance of wire electrical discharge machining process of Ni55.8Ti shape memory alloy, *Materials*, 2021, 14(10), doi: 10.3390/ma14102533.